UDC 622.834:334.45
DOI: 10.15587/1729-4061.2026.354698

ASSESSMENT OF THE BEARING CAPACITY OF RIGID SECONDARY SUPPORT SYSTEMS FOR GOB-SIDE RETAINED ENTRIES BASED ON STRAIN ENERGY ANALYSIS

Daria Chepiga
Corresponding author
PhD, Associate Professor
Ivano-Frankivsk Regional Training and Course Complex of Housing and Communal Services
S. Bandery str., 77, Ivano-Frankivsk, Ukraine, 76000
E-mail: daria.chepiha@donntu.edu.ua
ORCID: https://orcid.org/0000-0002-3331-9128
Leonid Bachurin
PhD, Associate Professor*
ORCID: https://orcid.org/0000-0003-2513-7284
Serhii Podkopaiev
Doctor of Technical Sciences, Professor**
ORCID: https://orcid.org/0009-0002-6051-4719
Danylo Polii
PhD Student*
ORCID: https://orcid.org/0009-0001-3374-815X
Olena Visyn
PhD, Associate Professor**
ORCID: https://orcid.org/0000-0003-2361-6708
Yevgen Podkopayev
Doctor of Philosophy (PhD)
Limited Liability Company Manufacturing Company Elteko
O. Tyhoho str., 2, Kostyantynivka, Donetsk region, Ukraine, 85105
ORCID: https://orcid.org/0009-0003-2217-3017
Halyna Herasymchuk
PhD, Associate Professor, Dean***
ORCID: https://orcid.org/0000-0002-1348-4927
Yaroslava Bachurina*
ORCID: https://orcid.org/0000-0001-6964-040X
*Department of Mining Management and Labor Protection
Donetsk National Technical University
Shevchenka str., 9, Drohobych, Ukraine, 82100
Department of Civil Security*
***Lutsk National Technical University
Lvivska str., 75, Lutsk, Ukraine, 43018

This study investigates deformation processes occurring in secondary support systems for gob-side retained entries in coal mine extraction panels mining thin seams. The task addressed is to stabilize gob-side retained entries by improving the bearing capacity of secondary support systems to prevent roof collapses and provide safe working conditions. The comparative assessment was conducted based on an analysis of strain energy-related indicators. Underlying the study are physical models simulating filling walls, concrete blocks, and combined structures consisting of blocks with wooden interlayers.

During uniaxial compression tests, the deformation capacity of each type of support system was determined; critical values of relative deformation at which the structures lose their functional performance were identified. The application of an energy-based approach has made it possible to quantify the stability limit and to predict the onset of structural failure. Experimental results showed that, under uniaxial compression, rigid secondary support systems operate under an increasing resistance mode before the initiation of failure processes. At the same time, the range of linear elastic deformation of the combined support structure is 33% greater than that of the homogeneous structure (damage initiation occurs at $\lambda_b = 0.103$ and $\lambda_b = 0.075–0.08$, respectively), which results in a delayed transition to loss of bearing capacity. The incorporation of limited yielding elements into rigid structures facilitates stress redistribution and enhances their deformation capacity.

An energy-based approach to analyzing the interaction between secondary support systems and the surrounding rock mass has been proposed, based on the use of strain energy density and its components, which characterize the processes of energy accumulation and dissipation. The practical significance of this study is associated with the application of the results to substantiate the design parameters for rigid secondary support systems for gob-side retained entries in coal extraction panels mining thin seams up to 1.2 m thick.

Keywords: entry support, bearing capacity, secondary support, deformation energy density, occupational safety

Received 16.12.2025
Received in revised form 27.02.2026
Accepted 11.03.2026
Published 30.04.2026

How to Cite: *Chepiga, D., Bachurin, L., Podkopaiev, S., Polii, D., Visyn, O., Podkopayev, Y., Herasymchuk, H., Bachurina, Y. (2026). Assessment of the bearing capacity of rigid secondary support systems for gob-side retained entries based on strain energy analysis. Eastern-European Journal of Enterprise Technologies, 2 (1 (140)), 13–24. https://doi.org/10.15587/1729-4061.2026.354698*

1. Introduction

To reduce roadway development during the preparation of extraction panels, as well as to completely dilute methane at the sources of its release, mining layouts with gob-side retained entries are used in the extraction areas of gassy mines. Such layouts allow the reuse of entries and create conditions for direct-flow ventilation. Common techniques for maintaining such entries do not always make it possible to ensure their proper operational condition. The solution to this problem

becomes especially important in the zone of influence of longwall operations, where unloading of the coal-rock mass occurs as a result of the extraction of a coal seam.

To ensure reliable maintenance of gob-side retained entries in the extraction areas, repair work is carried out, which includes the removal of fractured rock, re-supporting, and floor cutting. The volume of roadway repairs reaches 40–60% of the total length of the maintained entries, and complete re-supporting – 12–25% [1]. The labor intensity of maintaining the entries in extraction panels reaches 100 man-shifts per 1000 tons of average daily coal production [2]. Such operations complicate technological processes and are characterized by increased safety risks. At the same time, untimely restoration of the operational condition of maintained entries leads to a deterioration of extraction panel performance. In particular, this complicates ventilation and increases the costs of commissioning new extraction panels.

To prevent roof collapse and to ensure the maximum duration of the operation period without re-supporting, the selection of the technique for maintaining the gob-side retained entries is of great importance. Special attention should be paid to the type and parameters of secondary support structures built at the boundary with the gob. The operational condition of gob-side retained entries behind the longwall face is ensured by using secondary support structures with high bearing capacity. Such structures should provide effective resistance to lateral rock displacements, limit the movement of fractured rocks on the contour of the entries.

The issue in maintaining the operational condition of gob-side retained entries in the extraction panels of coal mines is the lack of a substantiated assessment of the bearing capacity of secondary support systems, taking into account their deformation capacity. The scientific relevance of the specified problem relates to the need to establish regularities governing the interaction between secondary support systems and the coal-rock mass during unloading. This could make it possible to improve existing and develop new measures to maintain entry stability, preventing roof collapses and reduce the volume of high-risk operations (repair and re-supporting of mine roadways).

2. Literature review and problem statement

The operational condition of supported gob-side retained entries in coal mines is ensured, along with the use of appropriate support, but also by the application of secondary support structures that reduce the negative impact of rock pressure on the surrounding coal-rock mass. Secondary support structures are constructed following the advance of the longwall face at the boundary with the gob area of the extraction panel. They perform the function of load-bearing structures, providing resistance to the converging movement of the undermined roof rocks that subside in the gob area, and the floor rocks that are heave due to unloading of the rock mass and stress redistribution within it. It is noted in [3] that most of pillarless techniques for maintaining gob-side retained entries require the construction of artificial load-bearing structures – secondary support structures. These are typically installed on the gob side (in stable and medium-stable rocks), while in weak rocks or when the roadway is driven with a wide entry – on both sides of the roadway. The disadvantage of this approach is its focus mainly on the force aspect of the performance of secondary support structures, which does not make it possible to consider the deformation and energy characteristics, load non-uniformity, and the effects of the combined action of secondary support structures with and the roadway support system. This limits the possibilities for a comprehensive assessment of the effectiveness of secondary support structures under actual operating conditions.

Protection of gob-side retained entries with filling walls consists in placing lightweight formwork between the rows of timber props and its subsequent filling with a fast-hardening water-mineral mixture [4]. The advantages of filling walls include the possibility of full mechanization of their construction. Pack walls are also used – the construction of which involves laying out packages with a dry fast-hardening cement-mineral mixture between the rows of timber props, followed by adding water to the mixture through a needle injector [4]. An obvious disadvantage of such secondary support structures is their unsuitability for performing load-bearing functions until the initial strength is reached and, accordingly, the significant influence of the setting rate of the hardening material on the bearing capacity of the structure, which is confirmed in studies [5, 6]. This disadvantage is absent in prefabricated high-strength structures – block reinforced concrete cribs (BRCCs), cribs made of slag concrete, aerated concrete, and concrete blocks. Concrete blocks are relatively brittle structures, which causes rapid failure of such load-bearing structures under dynamic loading. It was demonstrated in [7] that in the presence of wooden interlayers between the blocks, their bearing capacity increases significantly. The use of relatively thin, stiffer interlayers increases the crib bearing capacity by increasing the overall stiffness of the composite structure and localizing the splitting processes in the layers between the interlayers. In contrast, thick wooden interlayers give the structure limited yieldingness. The disadvantages of block concrete cribs as secondary support structures include the high cost and labor intensity of installation (only transportation is mechanized), as well as reduced durability under wetting conditions.

The stability of roadways is one of the key factors ensuring the safe and efficient conduct of underground mining operations. Conventional approaches to assessing the bearing capacity of secondary support structures are based mainly on force criteria. However, they do not take into account the energy nature of the processes that occur in the load-bearing structure under loading.

The use of energy-based indicators in rock deformation has recently acquired the status of a universal approach in the analysis of their strength characteristics [8–13]. At the same time, it should be taken into account that these methods are focused on assessing rock behavior in situ, so they involve laboratory testing of monolithic samples typically under triaxial compression conditions. In particular, in [8], the equivalent elastic modulus, proposed for the analysis of energy parameters of deformation, is determined by hysteresis cycles of loading-unloading. In the case of secondary support structures, which are often composite structures and retain their bearing capacity after partial failure, this approach loses its informativeness. In [9, 10], energy-based brittleness indices were proposed that take into account post-peak behavior and residual strength of rocks. However, these approaches are based on idealized unloading curves and a complete failure cycle of a monolithic specimen, which does not correspond to the behavior of composite secondary support structures (blocks, interlayers, filling elements). In [11], the energy-based indicator is integrated into a statistical damage model that requires

the determination of porosity, microdefect parameters, and effective pressure – which also goes beyond the scope of analysis of engineering structures under mine conditions. In [12], the energy evolution of sandstone after thermal exposure was investigated, but the results relate to thermally induced rock degradation and are not relevant to secondary support structures that are not subjected to high-temperature loading and do not always demonstrate the classic post-peak stage of brittle failure. At the same time, this confirms the universality of the energy-based approach as such. Study [13] summarizes mineralogical, elastic, and logging-based brittleness indices in the context of the analysis of the elastic properties of reservoir rocks and emphasizes that not only the composition and properties of rocks determine the failure behavior. It is also necessary to consider geomechanical parameters and loading conditions. In the case of secondary support structures, this conclusion encourages the use of indicators based on the integral characteristics of the deformation process – energy-based. Thus, the use of integral energy-based indicators determined from the stress-strain curve under uniaxial loading conditions is appropriate for analyzing the behavior of secondary support structures under load.

In studies [14–16], the assessment of the accumulation and release of strain energy in the rock mass is used to analyze the dynamics of stress redistribution around mine workings, complicated by rock anisotropy and the impact of mining operations. In these works, the use of energy-based indicators is typically limited to an integral assessment of deformation energy density without separating its components – elastic, dissipated, and fracture energy. In [14], the energy-based approach is used to describe the evolution of energy in the rock mass as the longwall face advances to substantiate the parameters of roadway support. However, this study is focused mainly on changes in the strain energy field within the surrounding rock mass of longwall and entries and does not extend to energy processes in secondary support structures. In [15], energy parameters were used to identify zones of plastic energy accumulation and potential failure, but the technique is focused on the analysis of large rock volumes and does not take into account the specific behavior of artificial structures with a predefined geometry and variable stiffness. In [16], the energy-based approach was integrated into a three-dimensional model of energy distribution around the roadway, but the emphasis was placed on rock mass behavior at different rates of roadway development, while the deformation characteristics of local load-bearing elements remained out of consideration. These studies confirm the effectiveness of the energy-based approach for analyzing the stress-strain state of rocks, but their results cannot be directly applied to assessing the bearing capacity of rigid secondary support structures.

When assessing the bearing capacity of support, energy indicators are used to optimize their parameters under rock pressure of varying intensity [17, 18]. The specific potential strain energy and its components, which characterize the ability of the material of secondary support structures to accumulate and dissipate energy during loading, are of key importance. This is important for determining the limits of the deformation capacity and defining the rational operating conditions for the application of the secondary support structures. The analysis of these indicators allows us to quantitatively determine the stability limit of secondary support structures and to predict the loss of their bearing capacity. In particular, the use of support capable of energy dissipation makes it possible to increase the roadways stability under conditions of large rock displacements by shifting the peak stress concentration deeper into the rock mass, as substantiated in [19, 20]. The results indicate that the energy-based deformation indicators, in particular strain energy density, reflect the internal work of systems and make it possible to assess not only the current state of load-bearing structures but also their ability to resist further destruction.

The effectiveness of controlling the condition of a gob-side retained entry depends on the ability of the secondary support structures to counteract rock pressure in the gob area. Under such conditions, the operational state of the gob-side retained entries depends on the bearing capacity of secondary support structures. The bearing capacity of secondary support structures changes during deformation, therefore its assessment should be based not only on deformation but also on energy-based characteristics that reflect the ability of structures to accumulate and dissipate the energy of rock pressure. This justifies the relevance of research aimed at evaluating the bearing capacity of secondary support structures taking into account the energy-based deformation indicators.

The application of results will make it possible to improve measures aimed at maintaining the stability of gob-side retained entries, preventing roof collapses, and ensuring safe working conditions for miners in entries supported behind the longwall face within extraction panels of coal mines.

3. The aim and objectives of the study

The aim of the study is to assess the bearing capacity of rigid secondary support structures based on the analysis of energy-related deformation indicators to prevent roof collapses and ensure the operational condition of gob-side retained entries within extraction panels of coal mines. This makes it possible to develop measures that prevent hazardous situations associated with mechanical injury to miners due to the unsatisfactory condition of the roadways, support failures, and rock falls.

To achieve the aim, the following tasks were set:

– to conduct experimental tests of models of homogeneous and combined rigid secondary support structures under uniaxial compression to determine the deformation capacity, critical values of relative deformation and energy indicators;

– to assess the deformation capacity of various structures (homogeneous and combined) based on a comparative analysis of energy and deformation characteristics to substantiate their effectiveness under conditions of coal-rock mass unloading.

4. The study materials and methods

The object of the study is the deformation processes occurring in secondary support structures of gob-side retained entries within the extraction panels of coal mines mining thin seams (up to 1.2 m thick).

The hypothesis of the study is as follows. The density of accumulated and dissipated strain energy of the secondary support structure determines its bearing capacity and stress-strain state under load. The maximum accumulation of strain energy occurs within the deformation capacity of the secondary support structure, which corresponds to the critical value of relative deformation.

The functional purpose of secondary support structures is to ensure the operational condition of gob-side retained

entries by reducing the intensity of lateral rock displacements, preventing roof collapse and deformation of roadway support. The secondary support structures under consideration perform the same function – ensuring the stability of gob-side retained entries. In view of this, they can be analyzed according to common deformation behavior criteria.

To assess the bearing capacity of secondary support structures and identify the features of deformation processes that manifest under incremental loading and affect the stability conditions of surrounding rocks, a study was conducted on experimental samples of sand-cement mixtures. This experiment is part of a comprehensive study of the deformation processes of secondary support structures to assess their bearing capacity [21–23].

Model No. 1 (filling wall): uniaxial compressive strength $\sigma_c = 34$ MPa, Poisson's ratio $\nu = 0.26$. Model No. 2 (concrete blocks): $\sigma_c = 36$ MPa, $\nu = 0.25$. Model No. 3 (concrete blocks with a wooden interlayer): $\sigma_c = 38$ MPa, $\nu = 0.27$. The experimental samples were installed between plates 0.08 m long, 0.04 m wide, and 0.02 m high, made of a sand-cement mixture with a compressive strength $\sigma_c = 38$ MPa. The geometric scale of the simulation is 1:25.

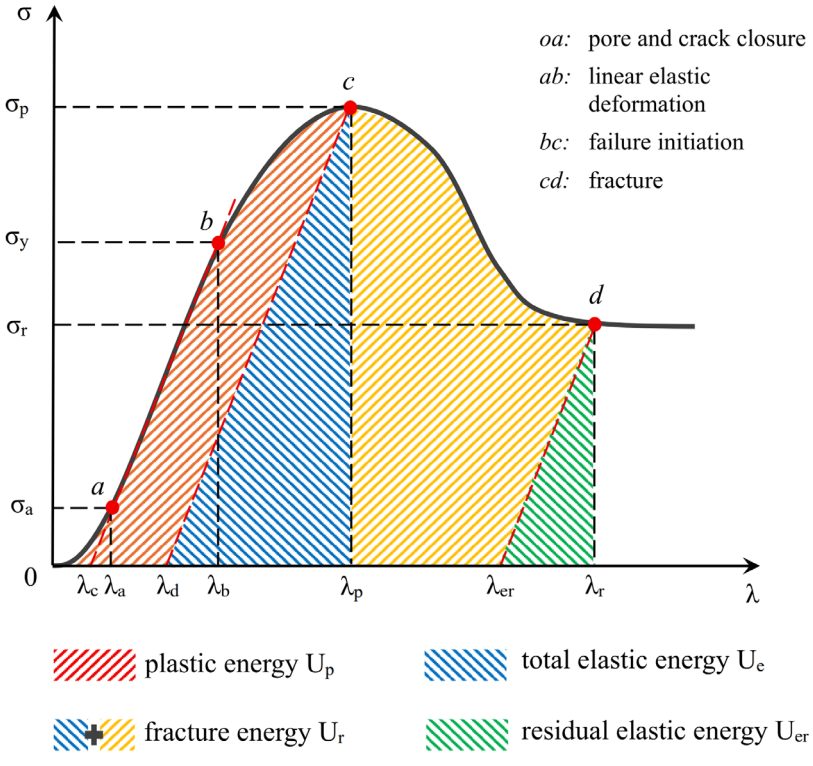

Fig. 1. Scheme of energy analysis of the stress-strain curve during compression of rocks and similar materials (adapted from [10, 11])

The size of the experimental samples was as follows: initial height $h_0 = 0.04$ m, cross-sectional area $S = 0.0016$ m^2, initial volume $V_0 = 0.000064$ m^3. The samples were represented in the form of a filling wall (model No. 1), and concrete blocks (models No. 2 and No. 3). Model No. 1 was monolithic. Model No. 2 consisted of two flat prismatic elements with a height of 0.02 m. Model No. 3 consisted of two flat prismatic elements with a height of 0.019 m, between which there was a thin wooden interlayer with a thickness of 0.002 m.

The loading conditions were simulated at a depth of 1000 m, which, with an average rock density of 2400 kg/m^3, corresponds to a pressure of 24 MPa. When testing the models, they were adjusted to ensure an equivalent level of loads. Deformation similarity under such conditions is achieved automatically since the initial parameter is a dimensionless indicator – relative deformation.

The experimental samples were placed between the metal plates of the GP-50 press and subjected to incremental loading. During the tests, at each stage of incremental loading, the deformation of the models Δh (m) and the corresponding load F (kN) were recorded. For simplicity, the deformation of the test equipment and friction forces were neglected.

The relative deformation λ of the experimental samples was determined from the following expression

$$\lambda = \frac{\Delta h}{h_0}, \tag{1}$$

where h_0 is the initial height of the sample, m.

To assess the bearing capacity of secondary support structures, an energy-based approach was used, which involves the analysis of the strain energy U and its components based on the change in mechanical stress and relative deformation [10, 11]. The analysis scheme of the stress-strain curve is shown in Fig. 1.

The total specific potential strain energy U (MJ/m^3) was determined as the area under the stress-strain curve using the trapezoidal method

$$U_i = \int_0^{\lambda_i} \sigma \, d\lambda \approx \sum_{i=1}^{n} \frac{\sigma_i + \sigma_{i-1}}{2} \left(\lambda_i - \lambda_{i-1}\right), \tag{2}$$

where σ is the mechanical stress, MPa.

The mechanical stress is equal to the pressure applied to the sample and is defined as the ratio of the load F (kN) to the cross-sectional area of the sample S (m^2)

$$\sigma = \frac{F}{S}. \tag{3}$$

The total specific potential strain energy represents the amount of energy that the structure can accumulate and dissipate per unit volume under loading. It is an important indicator of how the secondary support structure perceives the energy released as a result of stress redistribution in the rock mass around the mine roadway.

The elastic strain energy U_e (MJ/m^3) was determined by a relationship from [24], based on the assumption that the equivalent modulus of elasticity during unloading is equal to the initial modulus of elasticity E_d (MPa). At the same time, given that due to the nonlinearity of the stress-strain curve and the use of piecewise integration by the trapezoid method, slight discrepancies in the calculation results are possible. In the case when the calculated value U_e exceeds the value of the total energy U, it is taken as equal to U:

$$U_{ei} = \begin{cases} \dfrac{\sigma_i^2}{2E_d}, \text{ if } U_{ei} \le U_i, \\ U_i, \text{ if } U_{ei} > U_i. \end{cases} \tag{4}$$

The initial modulus of elasticity was determined from the linear section of the stress-strain curve (Fig. 1, section *ab*) using the functions of linear regression analysis in MS Excel (USA). The initial modulus of elasticity E_d, based on Hooke's law $E = \sigma/\lambda$, is equal to the angle of inclination of the linear regression line of section *ab* of the stress-strain curve.

Based on the results of analysis of the full stress-strain curve, a number of energy-based indicators are determined.

The total specific elastic strain energy absorbed by the sample, U_{te}, is determined from formula (4) for the peak stress value σ_p, which is achieved at a critical value of the relative strain λ_p

$$U_{te} = \frac{\sigma_p^2}{2E_d}. \quad (5)$$

The magnitude of plastic energy dissipation is due to irreversible material damage that occurs from the moment of transition from linear elastic deformation to elastoplastic (Fig. 1, section *bc*), and is equal to the difference between the total specific strain energy in the section 0-*a*-*b*-*c* (Fig. 1) and the total specific elastic strain energy U_{te}

$$U_p = \int_0^{\lambda_p} \sigma \mathrm{d}\lambda - U_{te}. \quad (6)$$

After reaching the critical level of relative deformation λ_p, the failure of the structure begins with the increase in deformation to the value λ_p (Fig. 1, section *cd*). After that, further evolution of the process occurs without increasing the load. The energy spent on this, or the fracture energy U_r, consists of the accumulated elastic energy and the additional energy spent on macroscopic failure. The fractured material has a residual strength, which is characterized by the value of the residual specific potential energy of deformation U_{er}. Therefore:

$$U_r = \int_{\lambda_p}^{\lambda_r} \sigma \mathrm{d}\lambda + U_{te} - U_{er}, \quad (7)$$

$$U_{er} = \frac{\sigma_r^2}{2E_d}. \quad (8)$$

Average increase in displacements, Δu_{avg}, m, was determined from the following formula

$$\Delta u_{avg} = \frac{\Delta u_i + \Delta u_{i-1}}{2}, \quad (9)$$

where Δu_{avg} – increase in displacements, m

$$\Delta u_i = \Delta h_i - \Delta h_{i-1}, \quad (10)$$

where i – measurement interval number.

The stiffness C (MN/m) of the experimental samples was determined as

$$C = \frac{F}{\Delta h}. \quad (11)$$

The bearing capacity of secondary support structures can be assessed based on an energy-based approach that takes into account the redistribution and transformation of strain energy during incremental loading [25]. To determine the deformation capacity of a secondary support structure, the elastic strain energy density coefficient η can be used

$$\eta = \frac{U_{te}}{U}, \quad (12)$$

which is equivalent to the brittleness coefficient of rocks proposed by Baron as the ratio of the work of deformation in the elastic region to the total work of fracture [26, 27].

The coefficient η reflects the part of the stored elastic energy in the total energy balance of the secondary support structure during its incremental loading under uniaxial compression. The smaller the safety margin from the moment of initiation of internal failure processes to the moment of loss of structural integrity, the closer the value of η is to 1. With an increase in the elastic strain energy density coefficient η, the share of elastic energy accumulated by the material of the structure increases, which indicates an increase in the bearing capacity of the secondary support structure within the deformation capacity and a limitation of its yieldingness.

5. Results of investigating the deformation behavior of rigid secondary support structures

5. 1. Results of experimental studies on the deformation of secondary support structure models under uniaxial compression

This chapter establishes the influence of deformation effects on the mechanical properties of models subjected to under uniaxial compression conditions under incremental loading.

Table 1 gives experimental data on incremental loading of model No. 1 under uniaxial compression conditions, which reproduce the deformation conditions of a filling wall.

Table 1

Experimental data on the incremental loading of model No. 1 under uniaxial compression conditions

F, kN	Δh, m	C, MN/m	Δu, m	Δu_{avg}, m	λ	σ, MPa	U_e, MJ/m^3	U, MJ/m^3	U_e/U
10	0.0009	11.11	0.0009	0.00045	0.023	6.25	0.04	0.072	0.601
15	0.0013	11.54	0.0004	0.00065	0.033	9.26	0.10	0.149	0.638
20	0.0014	14.29	0.0001	0.00025	0.035	12.29	0.17	0.171	0.977
25	0.0017	14.71	0.0003	0.0002	0.043	15.34	0.26	0.281	0.926
30	0.002	15.00	0.0003	0.0003	0.050	18.33	0.37	0.399	0.932
35	0.0023	15.22	0.0003	0.0003	0.058	21.29	0.50	0.558	0.899
40	0.0025	16.00	0.0002	0.00025	0.063	24.23	0.65	0.672	0.967
45	0.0028	16.07	0.0003	0.00025	0.070	27.18	0.82	0.852	0.960
50	0.003	16.67	0.0002	0.00025	0.075	30.07	1.00	0.995	1.006
60	0.011	5.45	0.008	0.0041	0.275	35.98	1.43	7.600	0.189
70	0.015	4.67	0.004	0.006	0.375	31.72	1.11	10.985	0.101
80	0.018	4.44	0.003	0.0035	0.450	31.25	1.08	13.346	0.081

Table 2 gives experimental data on the incremental loading of model No. 2 under uniaxial compression conditions, which reproduces the deformation conditions of concrete blocks.

Table 3 gives experimental data on incremental loading of model No. 3 under uniaxial compression conditions, which reproduces the deformation conditions of concrete blocks with a wooden interlayer.

Fig. 2 shows plots of change in the relative deformation λ of the models depending on the magnitude of the incremental load F (kN) under uniaxial compression.

Model No. 1. With an increase in load from 10 to 80 kN, the relative deformation increases from 0.023 to 0.45. A linear increase in relative deformation is observed in the range from 10 to 50 kN. The limit value of linear elastic deformation $\lambda_b = 0.075$.

Model No. 2. With an increase in load from 10 to 80 kN, the relative deformation increases from 0.02 to 0.425. A linear increase in relative deformation is observed in the range from 10 to 55 kN. The limit value of linear elastic deformation $\lambda_b = 0.08$.

Model No. 3. With an increase in load from 10 to 80 kN, the relative deformation increases from 0.025 to 0.35. A linear increase in relative deformation is observed in the range from 10 to 65 kN. The limit value of linear elastic deformation $\lambda_b = 0.103$.

Since models No. 1 (filling wall) and No. 2 (concrete blocks) differ essentially only in compressive strength, their behavior under load is very similar. In contrast, the combined model No. 3 (concrete blocks with a wooden interlayer) demonstrates a significantly different deformation pattern.

Fig. 3 shows plots of change in the model stiffness C (MN/m) versus relative deformation λ under incremental loading under uniaxial compression.

Model No. 1. In the elastic deformation range of the material, the stiffness increases from 11.1 to 16.7 MN/m. After the onset of macroscopic failure and loss of structural integrity, stiffness decreases sharply to 5.45 MN/m with a further decrease to 4.44 MN/m at a relative deformation of $\lambda = 0.45$.

Model No. 2. In the elastic deformation range of the material, the stiffness increases from 12.5 to 17.2 MN/m. After the onset of macroscopic failure and loss of structural integrity, stiffness decreases sharply to 5.0 MN/m with a further decrease to 4.7 MN/m at a relative deformation of $\lambda = 0.425$.

Model No. 3. In the elastic deformation range of the material, the stiffness increases from 10.0 to 15.85 MN/m. After the onset of macroscopic failure and loss of structural integrity, stiffness sharply decreases to 7.0 MN/m with a further decrease to 5.71 MN/m at a relative deformation $\lambda = 0.35$.

Table 2

Experimental data on the incremental loading of model No. 2 under uniaxial compression conditions

F, kN	Δh, m	C, MN/m	Δu, m	Δu_{avg}, m	λ	σ, MPa	U_e, MJ/m^3	U, MJ/m^3	U_e/U
10	0.0008	12.50	0.0008	0.0004	0.020	6.25	0.05	0.063	0.750
15	0.0011	13.64	0.0003	0.00055	0.028	9.28	0.10	0.125	0.833
20	0.0013	15.38	0.0002	0.00025	0.033	12.33	0.18	0.179	1.000
25	0.0016	15.63	0.0003	0.00025	0.040	15.37	0.28	0.276	1.000
30	0.0019	15.79	0.0003	0.0003	0.048	18.37	0.41	0.411	0.992
35	0.0022	15.91	0.0003	0.0003	0.055	21.34	0.55	0.550	1.000
40	0.0025	16.00	0.0003	0.0003	0.063	24.29	0.71	0.732	0.975
45	0.0028	16.07	0.0003	0.0003	0.070	27.22	0.90	0.912	0.982
50	0.0031	16.13	0.0003	0.0003	0.078	30.12	1.10	1.142	0.960
55	0.0032	17.19	0.0001	0.0002	0.080	32.99	1.21	1.205	1.000
60	0.012	5.00	0.0088	0.00445	0.300	35.94	1.56	8.787	0.178
70	0.015	4.67	0.003	0.0059	0.375	30.63	1.13	11.283	0.100
80	0.017	4.71	0.002	0.0025	0.425	31.25	1.18	12.830	0.092

Table 3

Experimental data on the incremental loading of model No. 3 under uniaxial compression conditions

F, kN	Δh, m	C, MN/m	Δu, m	Δu_{avg}, m	λ	σ, MPa	U_e, MJ/m^3	U, MJ/m^3	U_e/U
10	0.001	10.00	0.001	0.0005	0.025	6.25	0.04	0.078	0.567
15	0.0014	10.71	0.0004	0.0007	0.035	9.25	0.10	0.156	0.621
20	0.0018	11.11	0.0004	0.0004	0.045	12.26	0.17	0.263	0.647
25	0.002	12.50	0.0002	0.0003	0.050	15.24	0.26	0.332	0.792
30	0.0022	13.64	0.0002	0.0002	0.055	18.23	0.38	0.416	0.905
35	0.0025	14.00	0.0003	0.00025	0.063	21.21	0.51	0.573	0.889
40	0.0028	14.29	0.0003	0.0003	0.070	24.13	0.66	0.732	0.901
45	0.0031	14.52	0.0003	0.0003	0.078	27.03	0.83	0.937	0.883
50	0.0034	14.71	0.0003	0.0003	0.085	29.89	1.01	1.136	0.891
55	0.0036	15.28	0.0002	0.00025	0.090	32.73	1.21	1.292	0.939
60	0.0038	15.79	0.0002	0.0002	0.095	35.60	1.43	1.463	0.981
65	0.0041	15.85	0.0003	0.00025	0.103	38.45	1.67	1.759	0.951
70	0.01	7.00	0.0059	0.0031	0.250	41.21	1.92	7.614	0.253
80	0.014	5.71	0.004	0.00495	0.350	37.50	1.59	11.550	0.138

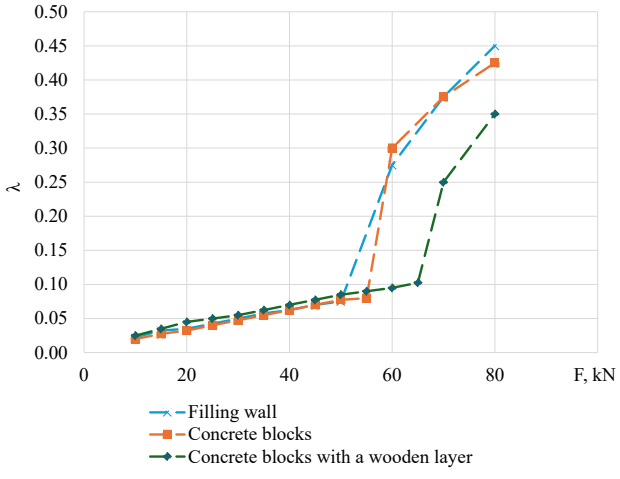

Fig. 2. Plots of relative deformation λ of the models depending on the load value F (kN)

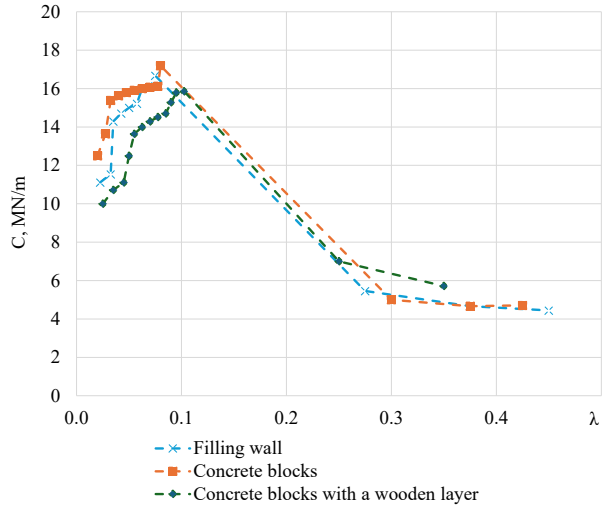

Fig. 3. Plots of model stiffness C (MN/m) depending on relative deformation λ

In all cases, at the initial elastic stage, an increase in stiffness and the presence of residual resistance of the failed structure are observed.

Fig. 4 shows plots of mechanical stress σ (MPa) versus relative deformation λ of the models during incremental loading under uniaxial compression.

All three models demonstrate similar behavior (Fig. 4): the presence of a nonlinear section or a section with a change in the deformation modulus at the beginning of the loading, followed by linear elastic deformation up to the peak uniaxial compressive strength. The ranges of purely elastic deformation sections used to determine the modulus of elasticity E_d, its value and the coefficient of determination of linear regression in the indicated sections are given in Table 4. The initial modulus of elasticity E_d characterizes the ability of the structure to accumulate elastic deformation energy. After the initiation of failure at point b (according to the scheme in Fig. 1), the secondary support structure does not completely lose its bearing capacity and is able to provide residual resistance, although further failure occurs practically without an increase in load. The critical relative deformation, upon reaching which the final loss of structural integrity occurs, is in the range of 0.25–0.3.

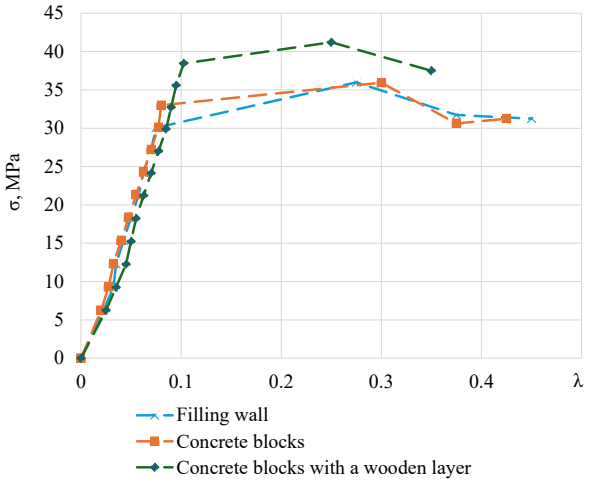

Fig. 4. Plots of mechanical stress σ (MPa) depending on relative deformation λ of the models

Table 4

Results of analyzing the initial linear section of the stress-strain curve

Model	λ_a	λ_b	E_d, MPa	r^2
No. 1. Filling wall	0.043	0.075	451.7	0.996
No. 2. Concrete blocks	0.020	0.078	413.6	0.998
No. 3. Concrete blocks with wood interlayer	0.045	0.103	441.6	0.996

Fig. 5 shows plots of average displacement increment Δu_{avg} (m) versus load on the models under uniaxial compression.

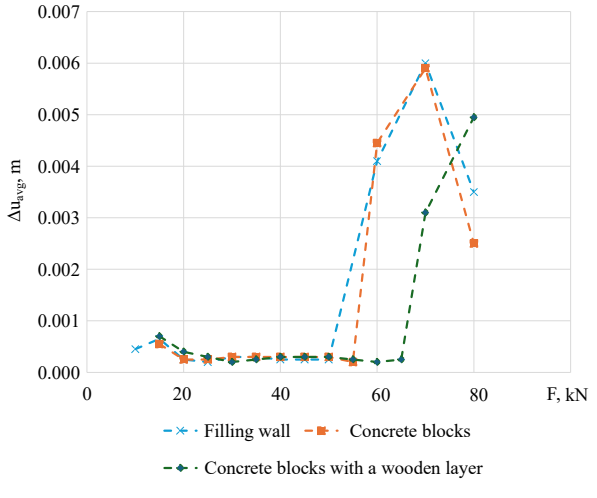

Fig. 5. Plots of average displacement increment Δu_{avg} (m) versus load F (kN) on the models

All three models of secondary support structures, due to the increase in stiffness (Fig. 3), demonstrate an increase in resistance within the linear elastic deformation range, which keeps the average displacement increment at an average level of 0.0003 m. A further sharp increase in the average displacement increment by an order of magnitude due structural failure is expected. At the same time, for the combined structure (model No. 3), this stage occurs later and at a higher load than in the case of homogeneous structures.

According to the stress-strain curve analysis scheme shown in Fig. 1 and experimental data (Tables 1–4, Fig. 2–5), the main

energy indicators of the deformation process of model samples were determined. The resulting data are given in Table 5.

Table 5

Key results of analyzing the stress-strain curves of model samples

Model	λ_p	σ_p, MPa	U_{te}, MJ/m^3	U_r, MJ/m^3	U, MJ/m^3	η
No. 1. Filling wall	0.275	36.0	1.43	3.71	10.99	0.19
No. 2. Concrete blocks	0.300	35.9	1.56	2.92	11.28	0.18
No. 3. Concrete blocks with wood interlayer	0.250	41.2	1.92	4.27	11.55	0.25

It was recorded that secondary support structures made of homogeneous materials (models No. 1 and No. 2) have similar characteristics of elastic energy accumulation – almost the same value of the coefficient η (0.19 and 0.18, respectively) and the absolute value of the total specific elastic strain energy accumulated until the final loss of structural integrity – 1.43 and 1.56 MJ/m^3, respectively. At the same time, in model No. 2, due to the greater dissipation of plastic strain energy at the stage of failure initiation, the fracture energy is less than in model No. 1 (2.92 and 3.71 MJ/m^3, respectively). In contrast, model No. 3 has a greater elastic strain energy density ($\eta = 0.25$) and at the same time dissipates more energy spent on structural failure (4.27 MJ/m^3).

5. 2. Results of evaluating the deformation capacity of rigid secondary support structures

This section reports the results of evaluating the deformation capacity of various structures (homogeneous and combined) based on a comparative analysis of energy and deformation characteristics to substantiate their effectiveness under the conditions of coal-rock mass unloading.

Fig. 6 shows plots of specific potential strain energy U (MJ/m^3) versus relative deformation λ of the models under uniaxial compression.

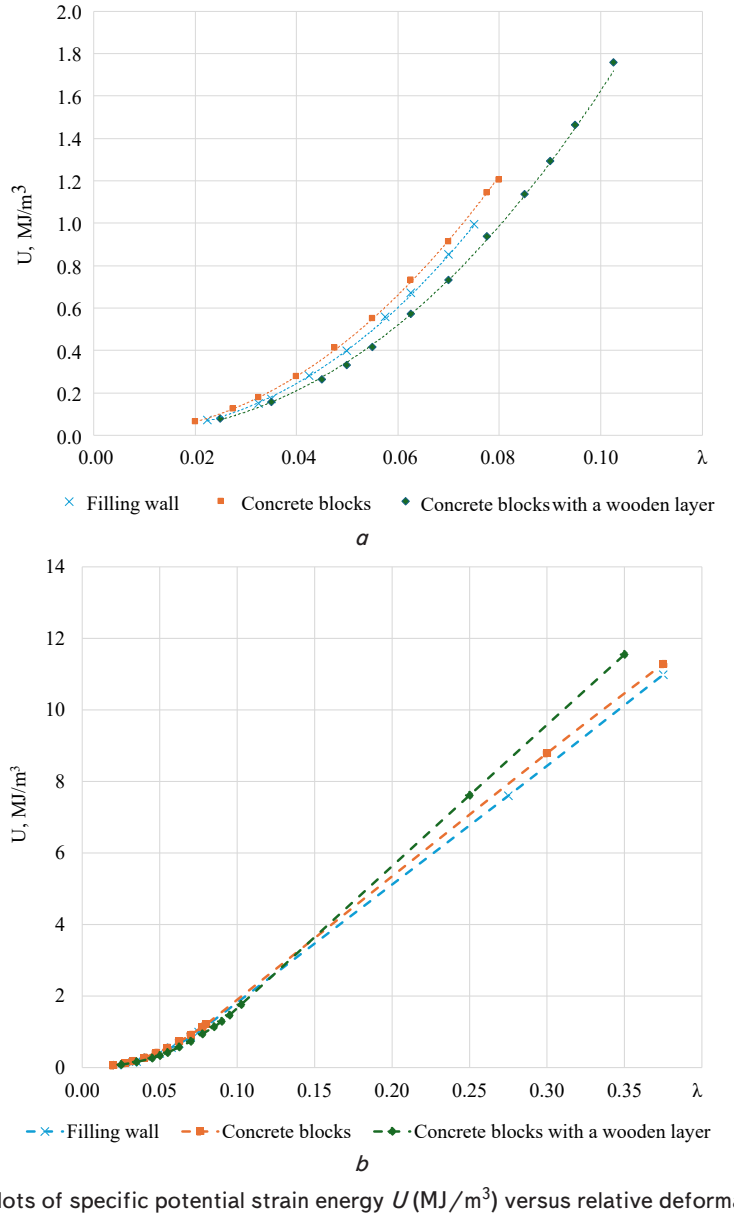

Fig. 6. Plots of specific potential strain energy U (MJ/m^3) versus relative deformation λ: *a* – within the deformation capacity; *b* – beyond the deformation capacity

Within the deformation capacity of secondary support structures, there is a power-law relationship of the form $U = m\lambda^n$ (Fig. 6, *a*) between the studied parameters, with the coefficients given in Table 6. This indicates the accumulation of strain energy in the material of the structure.

Table 6

Coefficients of the power-law regression relationship between the specific potential strain energy U (MJ/m^3) and the relative deformation λ within the deformation capacity

Model	m	n	r^2
No. 1. Filling wall	268.43	2.1347	0.9997
No. 2. Concrete blocks	314.79	2.2243	0.9997
No. 3. Concrete blocks with wood interlayer	276.3	2.2303	0.9997

Beyond the deformation capacity of the secondary support structures, there is a linear relationship between the change in the specific potential strain energy U and the relative deformation λ (Fig. 6, *b*) in the form $U = k\lambda + l$ with the parameters given in Table 7. At this stage, all additional energy applied to the sample is spent on its further rupture and failure.

Table 7

Parameters of the linear regression relationship between the specific potential strain energy U (MJ/m^3) and the relative deformation λ beyond the deformation capacity

Model	k	l	r^2
No. 1. Filling wall	33.261	–1.5113	1
No. 2. Concrete blocks	34.231	–1.5231	1
No. 3. Concrete blocks with wood interlayer	39.570	–2.2916	1

The plots in Fig. 6 reflect the ability of secondary support structures to accumulate strain energy (within the deformation capacity) and dissipate it (beyond the deformation capacity) during loading.

Fig. 7 shows plots of the elastic strain energy density coefficient η versus relative deformation λ of the models under uniaxial compression.

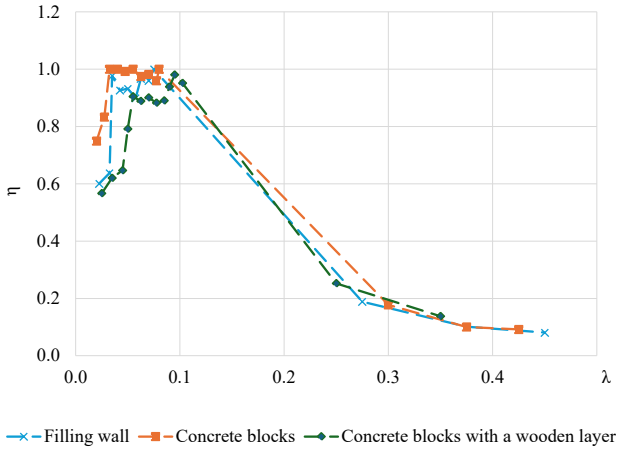

Fig. 7. Plots of elastic strain energy density coefficient η versus relative deformation λ of the models

The plots in Fig. 7 show that the stiffer homogeneous structures of models No. 1 and No. 2 are simultaneously more brittle (the coefficient η within the deformation capacity has a value close to unity). In contrast, model No. 3 is somewhat more yielding due to the presence of a wooden interlayer, which is able to deform itself and leads to a change in the failure mechanism of the blocks it separates (the mechanism of this phenomenon is described in [7]). Due to the ability to effectively accumulate energy and absorb deformations, the block structure with an interlayer has a wider deformation capacity, which is a favorably distinction from a filling wall or concrete blocks without interlayers.

The plots in Fig. 6, 7 shows how the elastic strain energy density of secondary support structures changes during uniaxial compression. They make it possible to assess the ability of the structure to accumulate and absorb energy at different stages of loading. The shape of the plots (Fig .6, 7) allows us to determine the ranges in which the secondary support structures work most effectively or lose their stability. These relationships also make it possible to perform a comparative analysis of structures of different designs in terms of their energy capacity.

6. Discussion of results of investigating the deformation behavior of rigid secondary support structures for assessing their deformation capacity

As a result of our studies, the deformation properties of secondary support structures have been established, which allows for comparative assessment of their bearing capacity. Secondary support structures were represented by homogeneous (filling wall, concrete blocks) and combined (2 concrete blocks with a wooden interlayer) models. The models were subjected to uniaxial compression under incremental loading. This condition simulated an incremental increase in the load on secondary support structures installed behind the longwall face. During the experiments, the load on the models and their relative deformation were recorded. The specific potential strain energy (2) was considered as the equivalent of the work spent on compression and irreversible deformations and failure of the models. The total specific elastic strain energy (5) determines the amount of energy accumulated by the structure until the moment of macroscopic failure. The process of elastic energy accumulation during loading was monitored by calculating the specific elastic strain energy at each stage of loading (4). For this purpose, the value of the initial modulus of elasticity was used, determined by linear regression analysis of section *ab* of the linear elastic deformation of the models (Fig. 1, 4, Table 4). The total energy capacity for the failure of the structure includes the accumulated elastic strain energy and the additional energy required to create additional surfaces (6). The elastic strain energy density of the secondary support structure was determined by the ratio of the accumulated specific elastic strain energy to the total specific potential strain energy (12). This indicator is an energy-based representation of the change in the stiffness of secondary support structures under incremental loading when there are simultaneous accumulation and dissipation of energy. Beyond the deformation capacity of secondary support structures, the accumulated energy is spent on failure. At the same time, after the loss of structural integrity, secondary support structures retain a certain residual bearing capacity due to the need to expend additional energy on further fracture of the material.

As part of our experiment, it was demonstrated using models that homogeneous structures have a narrower range

of deformations, within which the linear elastic stage of deformation is realized, which determines the initial operation of the secondary support structure in the increasing resistance mode $\lambda \leq 0.075–0.08$. In contrast, a structure made of the same material but divided into separate layers by introducing a wooden interlayer of limited yield (its thickness is equivalent to using 5 cm thick boards on a real scale), has on average a 33% greater deformation capacity ($\lambda \leq 0.103$). It is in this interval that the accumulation of most of the elastic strain energy occurs. The increase in displacements is insignificant (Tables 1–3, Fig. 2, 4, 5). This makes it possible to limit movements during incremental loading and avoid collapses. Within the deformation capacity of secondary support structures ($\lambda \leq 0.075–0.103$), an increase in their stiffness and a decrease in the average displacement increment are observed (Fig. 3, 5).

Beyond the deformation capacity of secondary support structures at $\lambda > 0.075–0.103$, their bearing capacity is lost. Initially, part of the energy is dissipated through micro-fracturing, which causes an increase in displacements with a small increase in load. Failure is characterized by a decrease in stiffness, irreversible changes in shape when the structural integrity is lost (Tables 1–3). After the loss of structural integrity (macroscopic failure), the average displacement increment increases simultaneously with an increase in the mechanical work of compression, which is spent on further fracture (Fig. 5, 6). A clear difference in the mechanisms of strain energy redistribution is illustrated by the presence of a power-law relationship between the specific potential elastic strain energy and the relative deformation within the deformation capacity (Fig. 6, *a*; Table 6) and a linear relationship beyond the deformation capacity (Fig. 6, *b*; Table 7).

At the same time, unlike building structures, for secondary support structures of gob-side retained entries, the loss of structural integrity is not catastrophic. Due to the limited space at the location of the secondary support structures, as well as the relatively slow process of roof-to-floor convergence, residual resistance becomes of significant importance. The elastic strain energy density coefficient η allows us to estimate both the initial strength characteristics of the secondary support structure within the deformation capacity and the value of residual resistance, which is proportional to the ratio of the accumulated and total strain energy. According to the results of the analysis of the full stress-strain curves of model samples, it was established that within the deformation capacity of secondary support structures, the elastic strain energy density coefficient η (Table 5) for the filling wall (model No. 1) is 0.19. In concrete blocks without a wooden interlayer (model No. 2) $\eta = 0.18$, and in the combined structure of blocks with a wooden interlayer (model No. 3) $\eta = 0.25$. The absolute value of the total specific elastic strain energy accumulated until the final loss of structural integrity for models No. 1 and No. 2 is 1.43 and 1.56 MJ/m^3, respectively. At the same time, in model No. 2, due to the greater dissipation of plastic strain energy at the stage of failure initiation, the fracture energy is less than in model No. 1 (2.92 and 3.71 MJ/m^3, respectively). In contrast, model No. 3 has a higher elastic strain energy density ($\eta = 0.25$) and at the same time dissipates more energy spent on structural failure (4.27 MJ/m^3). These differences indicate that the combined structure with a wooden interlayer provides the highest energy absorption efficiency.

The extended deformation capacity of the combined structure and the change in its destruction mechanism affect the ability to effectively accumulate energy and absorb deformations. Such a mode of operation allows the secondary support structure to dissipate part of the external energy and postpone the transition from the elastic to the plastic state while maintaining a relatively higher level of resistance, ensuring the stability of the entries. A secondary support structure with a wider deformation capacity, interacting with roof and floor, plays the role of an energy-absorbing barrier, that provides a damping effect during the stage of intensive coal-rock mass unloading.

Data from the analysis of the stress-strain curves of secondary support structures (Table 5, Fig. 6, 7) are an informative tool for assessing the energy-absorbing capacity of secondary support structures. They make it possible to characterize the processes of energy accumulation, identify critical states associated with the exhaustion of the bearing capacity of secondary support structures. This creates a basis for optimizing design solutions for their improvement and adaptation to specific application conditions. It can be assumed that the yielding of secondary support structures directly affects the energy indicators of their deformation, since it changes the balance of accumulated and dissipated strain energy. Combining yielding elements with rigid ones allows for a purposeful change in the strength characteristics of secondary support structures. The bearing capacity of secondary support structures from the standpoint of energy indicators of deformation is determined by their ability to accumulate and dissipate energy that is released in the rock mass around the supported entry as a result of stress redistribution. Energy characteristics – components of the specific potential strain energy and the elastic strain energy density coefficient, make it possible to quantitatively assess the deformation capacity limit of a secondary support structure, the moment of loss of its bearing capacity and the nature of stiffness changes. By analyzing these indicators, it is possible to assess the extent to which a supporting structure is able to accumulate potential energy without entering the failure stage, which is key to ensuring the reliability and safe operation of gob-side retained entries.

The fundamental difference of our results is the adaptation of the energy approach, conventionally applied to monolithic rocks [8–13] and rock masses [14–16], for the analysis of rigid and combined secondary support structures. In the mentioned works, energy indicators are used mainly for the integral assessment of the strain energy density [14–16] or for the optimization of the support parameters according to the force and energy criteria [17–20]. In contrast, in this study, the components of the energy balance of secondary support structures are determined and the limit of their deformation capacity is quantitatively established. The transition from the conventional strength assessment to the energy analysis of the deformation process is justified, which made it possible to establish the regularities of energy redistribution at different stages of loading. The increase in energy capacity and residual bearing capacity of the combined secondary support structure compared to homogeneous models is experimentally confirmed.

It is also worth noting the limitations of the proposed approach. The study focuses on rigid homogeneous and combined structures that retain their bearing capacity after partial failure. This behavior is significantly different from monolithic rock samples, for which energy criteria have conventionally been devised. Accordingly, the use of classical energy indicators required adaptation, and the results obtained are valid only for structures that demonstrate a similar nature of deformation. Therefore, the approach is acceptable specifically

for comparative analysis of the bearing capacity of secondary support structures, and scaling this methodology to full-scale structures requires additional validation. This requires in-situ observations of the deformation of secondary support structures with different geometric parameters, taking into account technological deviations during construction and interaction with different types of roadways support.

A limitation of the research is the scale of laboratory modeling and simplified conditions of uniaxial loading without taking into account the scale effect and the interaction of secondary support structures with the surrounding rock mass and primary support. The influence of the scale effect was not specifically analyzed within the framework of this work, which makes it advisable to further test models of different sizes. This also requires conducting in-situ experiments and studying the interaction of secondary support structures in a complex stress-strain state using an expanded experimental base.

It is advisable to focus further research on taking into account the influence of various combinations of block elements with rigid and yielding interlayers on the bearing capacity and deformation capacity of secondary support structures, as well as assessing the dependence of their energy capacity on the loading rate.

7. Conclusions

1. Analysis of the energy balance of rigid secondary support structures allows us to estimate their deformation capacity, which is characterized by the limits of the range of linear elastic deformation, the ability to effectively accumulate and dissipate strain energy, and the residual bearing capacity after failure. It has been determined that under uniaxial compression, rigid secondary support structures operate in an increasing resistance mode prior to the initiation of failure. Experimental results show that a combined secondary support structure, formed from rigid blocks with a yielding wooden interlayer between them, demonstrates significant operational differences compared to homogeneous block and monolithic structures. Specifically, this design expands the linear elastic range by 33%. The loss of bearing capacity in the combined structure occurs at a higher relative deformation ($\lambda_b = 0.103$) compared to homogeneous ones ($\lambda_b = 0.075–0.08$).

2. It has been substantiated that a block structure divided by a yielding wooden interlayer possesses greater deformation capacity due to its ability to accumulate and dissipate a larger amount of energy compared to homogeneous structures, while also maintaining higher residual resistance. The ability of secondary support structures to accumulate energy is evaluated using the elastic strain energy density coefficient η, which determines the ratio of the elastic strain energy accumulated within the structure's volume to the total specific potential strain energy. This coefficient characterizes the ability of a secondary support structure to accumulate and dissipate energy within its deformation capacity, thereby effectively accommodating rock pressure.

Conflicts of interest

The authors declare that they have no conflicts of interest in relation to the current study, including financial, personal, authorship, or any other, that could affect the study and the results reported in this paper.

Funding

The study was conducted without financial support.

Data availability

All data are available in the main text of the manuscript.

Use of artificial intelligence

The authors confirm that they did not use artificial intelligence technologies when creating the current work.

Acknowledgments

The authors express their gratitude to the defenders of Ukraine for the opportunity to continue working and to engage in scientific and teaching activities during the war.

Authors' contributions

Daria Chepiga: Conceptualization, Investigation, Writing – original draft; **Leonid Bachurin**: Methodology, Formal analysis, Writing – review & editing; **Serhii Podkopaiev**: Resources, Conceptualization, Formal analysis, Writing – original draft; **Danylo Polii**: Investigation; **Olena Visyn**: Writing – original draft; **Yevgen Podkopayev**: Resources; **Halyna Herasymchuk**: Validation; **Yaroslava Bachurina**: Visualization.

References

1. Sheka, I. V. (2024). Obgruntuvannia ratsionalnykh parametriv kriplennia iz kompozytnykh materialiv dlia hirnychykh vyrobok vuhilnykh shakht, shcho roztashovani na hlybynakh ponad 1000 metriv. Dnipro: Natsionalnyi tekhnichnyi universytet "Dniprovska Politekhnika", 158. https://doi.org/10.13140/RG.2.2.18898.77765
2. Kyrychenko, V. Ya., Usachenko, B. M. (2008). Driftic metal timbers, answering to economic requirements and geomechanical problems of the big depths. Heotekhnycheskaia Mekhanyka, 78, 178–189. Available at: http://www.geotm.dp.ua/index.php/en/collection/474-geo-technical-mechanics-2008/geo-technical-mechanics-2008-78/7562-2024-06-04-19-42-58
3. Bondarenko, V. I., Buzylo, V. I., Tabachenko, M. M., Medianyk, V. Yu. (2010). Heomekhanichni osnovy pidvyshchennia stiykosti pidhotovchykh vyrobok. Dnipropetrovsk: Natsionalnyi hirnychyi universytet, 408. Available at: http://ir.nmu.org.ua/handle/123456789/156064
4. Pro zatverdzhennia Instruktsiyi z zabezpechennia stiykosti dilnychnykh vyrobok dlia povtornoho vykorystannia na vuhilnykh shakhtakh. Ministerstvo Enerhetyky Ukrainy nakaz 10.11.2022 No. 378. Available at: https://zakon.rada.gov.ua/laws/show/z1665-22

5. Yalanskiy, A. O., Slashchov, I. M., Slashchova, O. A., Seleznov, A. M., Arestov, V. V. (2018). Development of new auxiliary measures for protecting preparatory roadways by the cast strips. Geo-Technical Mechanics, 141, 3–17. https://doi.org/10.15407/geotm2018.141.003
6. Li, H., Zu, H., Zhang, K., Qian, J. (2022). Study on Filling Support Design and Ground Pressure Monitoring Scheme for Gob-Side Entry Retention by Roof Cutting and Pressure Relief in High-Gas Thin Coal Seam. International Journal of Environmental Research and Public Health, 19 (7), 3913. https://doi.org/10.3390/ijerph19073913
7. Kanin, V. O., Antsyferov, A. V. (2004). Okhorona hirnychykh vyrobok hazobetonnym kriplenniam. Donetsk: TOV "Alan", 396.
8. Qin, T., Wang, Y., Hou, X., Duan, Y. (2023). A characterization method for equivalent elastic modulus of rock based on elastic strain energy. Frontiers in Earth Science, 11. https://doi.org/10.3389/feart.2023.1120344
9. Gong, F., Wang, Y. (2022). A New Rock Brittleness Index Based on the Peak Elastic Strain Energy Consumption Ratio. Rock Mechanics and Rock Engineering, 55 (3), 1571–1582. https://doi.org/10.1007/s00603-021-02738-y
10. Rahimzadeh Kivi, I., Ameri, M., Molladavoodi, H. (2018). Shale brittleness evaluation based on energy balance analysis of stress-strain curves. Journal of Petroleum Science and Engineering, 167, 1–19. https://doi.org/10.1016/j.petrol.2018.03.061
11. Liu, Z., Fan, T., Wang, Z., Yang, R., Fan, H., Wang, H., Hu, N. (2025). A rock brittleness evaluation method in interbedded reservoirs based on statistical damage constitutive. Journal of Petroleum Exploration and Production Technology, 15 (7). https://doi.org/10.1007/s13202-025-02008-5
12. Qiao, L., Hao, J., Liu, Z., Li, Q., Deng, N. (2022). Influence of temperature on the transformation and self-control of energy during sandstone damage: Experimental and theoretical research. International Journal of Mining Science and Technology, 32 (4), 761–777. https://doi.org/10.1016/j.ijmst.2022.02.008
13. Krasnikova, O., Kuzmenko, P., Vyzhva, S. (2024). Analysis of the methods of determining the brittleness index and their application for terrigenous reservoir rocks of the Dnipro-Donetsk Basin. Visnyk of Taras Shevchenko National University of Kyiv. Geology, 1 (104), 22–29. https://doi.org/10.17721/1728-2713.104.03
14. Li, L., Li, G., Gong, W., Wang, J., Deng, H. (2019). Energy Evolution Pattern and Roof Control Strategy in Non-Pillar Mining Method of Goaf-Side Entry Retaining by Roof Cutting – A Case Study. Sustainability, 11 (24), 7029. https://doi.org/10.3390/su11247029
15. Hui, Z.-L., Zhao, Z.-Q., Wei, X.-X., Yao-Li. (2025). The energy and stress evolution law of surrounding rock in gob side entry driving of adjacent mining faces. Scientific Reports, 15 (1). https://doi.org/10.1038/s41598-025-10977-0
16. Xin, X., Meng, Q., Pu, H., Wu, J. (2024). Theoretical analysis and numerical simulation analysis of energy distribution characteristics of surrounding rocks of roadways. Tunnelling and Underground Space Technology, 147, 105747. https://doi.org/10.1016/j.tust.2024.105747
17. Wang, C., Liu, L., Elmo, D., Shi, F., Gao, A., Ni, P., Zhang, B. (2018). Improved energy balance theory applied to roadway support design in deep mining. Journal of Geophysics and Engineering, 15 (4), 1588–1601. https://doi.org/10.1088/1742-2140/aab3a0
18. Huang, S., Li, Z. (2023). Optimization and Application of Coal Pillar in Fully Mechanized Mining Face based on Energy Analysis. International Journal of Energy, 3 (3), 47–51. https://doi.org/10.54097/ije.v3i3.011
19. Wang, W., Qiu, W. (2023). Energy-Dissipation Support Technology for Large Deformation Tunnels Based on the Post-Peak Behavior of Steel Plate Buckling: A Case Study. Applied Sciences, 13 (21), 11972. https://doi.org/10.3390/app132111972
20. Liu, X., Zhang, Y., Fan, D., Zhao, Y., Gao, Y., Pei, H., Shi, Z. (2025). Energy driven mechanism of surrounding rock deformation and failure of mining roadway and classified control technology. Scientific Reports, 15 (1). https://doi.org/10.1038/s41598-025-98452-8
21. Chepiga, D., Bessarab, I., Hnatiuk, V., Tkachuk, O., Kipko, O., Podkopaiev, S. (2023). Deformation as a process to transform shape and volume of protective structures of the development mine workings during coal-rock mass off-loading. Mining of Mineral Deposits, 17 (4), 1–11. https://doi.org/10.33271/mining17.04.001
22. Bachurin, L. L., Iordanov, I. V., Bessarab, I. M., Korol, A. V., Kaiun, O. P., Podkopaiev, Y. S. et al. (2021). Comprehensive research of the stability of haulage drifts on steep coal seams in different protection methods. Visnyk Natsionalnoho universytetu vodnoho hospodarstva ta pryrodokorystuvannia, 1 (93), 217–236. Available at: https://ep3.nuwm.edu.ua/22666/
23. Chepiga, D., Podkopaiev, S., Kayun, O., Bielikov, A., Podkopayev, Y., Kipko, O., Pidhurna, O. (2024). Assessing the stability of protective structures in preparatory mining workings under conditions of static load. Eastern-European Journal of Enterprise Technologies, 3 (1 (129)), 57–68. https://doi.org/10.15587/1729-4061.2024.304721
24. Sadd, M. H. (2009). Elasticity. Academic Press, 536. https://doi.org/10.1016/b978-0-12-374446-3.x0001-6
25. Lu, G., Yu, T. (2003). Energy absorption of structures and materials. Woodhead Publishings, 403. https://doi.org/10.1533/9781855738584
26. Baron, L. I., Kurbatov, V. M. (1959). O diagramme szhatiya krepkih gornyh porod. Nauchnye Soobsheniya IGD AN SSSR, 22.
27. Hucka, V., Das, B. (1974). Brittleness determination of rocks by different methods. International Journal of Rock Mechanics and Mining Sciences & Geomechanics Abstracts, 11 (10), 389–392. https://doi.org/10.1016/0148-9062(74)91109-7